CHAPTER IV
ELECTRORHEOLOGICAL PROPERTIES OF PERCHLORIC ACID-DOPED POLYTHIOPHENE SUSPENSIONS

4.1 Abstract

Poly(3-thiophene acetic acid), PTAA, was synthesized via an oxidative polymerization and doped with perchloric acid to control its conductivity. Rheological properties of the $HClO_4$ doped PTAA/silicone oil suspensions were measured in oscillatory shear to investigate the effects of electric field strength, particle concentration, and particle conductivity on ER characteristics. The PTAA based ER fluids exhibit viscoelastic behavior under an applied electric field and the ER response is amplified with increase of electric field strength. The dynamic moduli, G' and G", increase dramatically by 10 orders of magnitude, when the field strength is increased to 2 kV/mm. The suspensions exhibit a transition from fluid-like to solid-like behavior as the field strength increased, and reach a saturated ER response at a field strength of 1 kV/mm. Increase of particle concentration and particle conductivity result in a lower transition field strength. Scaling arguments are presented which successfully superpose the scaled moduli at various electric field strengths onto a single master function of the dimensionless frequency.

KEYWORDS: Electrorheological fluid, Conductive polymer, Polythiophene, Perchloric acid

4.2 Introduction

Electrorheological (ER) fluids are suspensions that exhibit a dramatic change in rheological properties in the presence of AC or DC electric fields. Commonly, they are composed of polarizable particles dispersed in a non-conducting fluid. Upon the application of an electric field, chain-like or fibrillar aggregates of the suspended particles are oriented along the direction of the electric field, thereby inducing viscoelasticity and a drastic increase in viscosity (Sakurai, 1999). The ability of these materials to transform electrical energy into mechanical energy has motivated research and development into various technological applications, as the active elements of clutches, breaks, shock absorbers, engine mounts, valves, and flow pumps (Voyles *et al.*, 1996, Kamath and Wereley, 1997, Mavroidis *et al.*, 2000). Typically, the steady state rheological properties have been investigated for most ER fluids. The dynamic rheological responses, which probe the equilibrium structure of these materials in the presence and absence of the applied field, have not been studied so extensively (Parthasarathy and Klingenberg, 1999, Chin and Winter, 2002, Ha and Yang, 2000, Mcleish *et al.*, 1991, Jordan *et al.*, 1992).

Recently, there has been interest in using conductive polymers as suspended particles for dry-base ER fluids. Conductive polymers can offer a variety of advantages for ER systems: better thermal stability, insolubility, and more controllable viscosity. Suspensions of conductive polymers exhibit intrinsic ER properties without the necessity to introduce other additives. The polarization is induced by the motion of electrons within the suspended particles under application of electric field. Various conductive polymers have been tested as particulate materials in ER systems. Examples include polyaniline (PANI) and its derivatives [Jang *et al.*, 2001, Kim *et al.*, 2000, Lee *et al.*, 1999, Krause and Katerine, 2001, Lee *et al.*, 1998), PANI copolymers (Lee *et al.*, 2001, Cho *et al.*, 2000, Jun *et al.* , 2002, Choi *et al.*, 2001), polypyrrole (Kim and Park, 2002, Goodwin *et al.*, 1997), poly (acene quinone) radical (Choi *et al.*, 2001), poly (napthalene quinone) radical (Cho and Choi, 2000), and poly (p-phenylene) (Choi *et al.*, 2001, Sim *et al.*, 2001).

In this study, we explore the ER behavior of Poly (3-thiophene acetic acid) (PTAA), doped with perchloric acid ($HClO_4$) to vary the conductivity. The dynamic

moduli of $HClO_4$-doped PTAA suspensions were investigated in the presence and absence of applied electric fields. The effect of field strength, mechanical deformation frequency, doping degree (conductivity values), and particle concentration on the moduli were investigated and compared with existing theory.

4.3 Experimental

4.3.1 Materials

3-thiopheneacetic acid, 3TAA (AR grade, Fluka) was used as the monomer. Anhydrous ferric chloride, $FeCl_3$ (AR grade, Riedel-delHean) was used as the oxidant. Chloroform, $CHCl_3$ (AR grade, Lab-Scan) and methanol, CH_3OH (AR grade, Lab-Scan) were dried over CaH_2 for 24 hours under the nitrogen atmosphere and then distilled. The perchloric acid dopant, $HClO_4$ (AR grade, AnalaR) was used as received. The dispersing phase was silicone oil (AR grade, Dow corning) with density 0.96 g/cm^3 and kinematic viscosity of 100 cSt, and was vacuum-dried and stored in a dessiccator prior to use.

4.3.2 Polymerization Procedure

Poly (3-thiopheneacetic acid), PTAA was synthesized by oxidative-coupling polymerization according to the method of Kim *et al.* (Kim *et al.*, 1999). 10.0 g of 3-thiopheneacetic acid was refluxed for 24 hours in 50 ml of dry methanol with 1 drop of concentrated H_2SO_4, to protect against the oxidative decomposition of the carboxylic acid group of monomer during polymerization. The methanol was evaporated, and the residue was extracted with diethyl ether. The extract was washed with deionized water, dried with anhydrous $MgSO_4$, and then filtered. The diethyl ether was evaporated from the filtrate by rotating evaporator.

A solution of 10 mmol of protected monomer in 20 ml of chloroform was added dropwise to a solution of 40 mmol of ferric chloride in 30 ml of chloroform under nitrogen atmosphere. The reaction was carefully maintained at 0 $^{\circ}C$ ($\pm$ 0.5 $^{\circ}C$) for 24 hours. The reaction mixture was precipitated, by pouring into a large excess amount of methanol. The precipitate was repeatedly washed with methanol and deionized water. The precipitate was hydrolyzed, by heating 0.5 g

precipitate in 50 ml of 2.0 M NaOH solution for 24 hours at 100 °C. The PTAA obtained was neutralized and precipitated with a dilute HCl solution. The PTAA was washed several times with deionized water before vacuum drying at room temperature for 2 days.

To examine the effect of particle conductivity on the electrorheological properties, PTAA particles having different conductivity values were prepared by doping with perchloric acid (Chen *et al.*, 2000). The $HClO_4$ doped PTAA was prepared by stirring ground PTAA (~7.04 mmol) with $HClO_4$ aqueous solution at room temperature for 3 days. The amounts of acid used were 7.04 ml of ~0.1 M aqueous acid and 176 ml of ~ 4.0 M aqueous acid for low and high doping ratios of 1.09×10^{-3} and 0.255, respectively. The $HClO_4$ doped PTAA particles were filtered and vacuum-dried for 24 hours before grinding with a mortar and pestle and then passed through a 38 μm sieve shaker to control the particle size distribution.

4.3.3 Preparation of ER fluids

The electrorheological, ER, fluids were prepared by dispersing $HClO_4$ doped PTAA particles in silicone oil (density 0.96 g/cm^3 and kinematic viscosity 100 cSt) with ultrasonicator for 30 minutes at 25 °C. The prepared ER fluids were then stored in a dessiccator prior to use and redispersed before each measurement.

4.3.4 Characterization Methods

Fourier Transform Infrared (FT-IR) spectra were obtained using a FT-IR spectrometer (Bruker, Equinox 55/FRA 1065) operated in the transmission mode with 32 scans and a resolution of ± 4 cm^{-1}, covering a wavenumber range of 4000-400 cm^{-1} using a deuterated triglycine sulfate detector. Optical grade KBr (Carlo Erba Reagent) was used as the background material. The synthesized PTAA was intimately mixed with dried KBr at a ratio of PTAA:KBr = 1:20.

^{1}H-NMR spectra in solution state were recorded at 25 ± 1 °C using a 300 MHz Digital NMR spectrometer (Bruker, DPX-300). Deuterated dimethyl sulfoxide was used as the standard solvent.

The UV-Visible spectrum of the synthesized PTAA powder, dissolved in DMSO, was recorded with a UV-Vis spectrometer (Perkins Elmer, Lambda 10), at a scan speed of 240 mm/min, and a slit width of 2.0 nm, using a deuterium lamp as the light source, at wavelengths between 190-800 nm.

The thermal stability of PTAA was investigated using a thermogravimetric analyzer (Perkin Elmer, TGA7) in the temperature range 25 to 750 °C at a heating rate of 10 °C/min.

The particle size distribution of PTAA powder was determined using a particle size analyzer (Malvern, Master Sizer X).

Scanning electron micrographs were taken with a scanning electron microscope (JEOL, JSM-5200-2AE) using an acceleration voltage of 20 kV and a magnification of 1,000.

4.3.5 Specific Conductivity Measurement

To determine the electrical conductivity, $HClO_4$ doped polythiophene disks (25 mm diameter and ~0.2 mm thickness) were prepared by molding with a hydraulic press. Electrical conductivity was measured using a custom-built four-point probe. The specific conductivity, σ (S/cm), was obtained, by measuring the resistance, R and using the following relation: $\sigma = (1/Rt)(1/K)$, where t is the film thickness and K is the geometric correction factor. A geometric correlation factor was calibrated by using standard silicon wafer sheets with known specific resistivity values. The measurements were performed in the linear Ohmic regime i.e. the specific conductivity values were independent of the applied DC current. The measurements were carried out at 27 °C and repeated at least two times.

4.3.6 Electrorheological Properties Measurement

A fluids rheometer (Rheometrics, ARES) was used to investigate the rheological properties. It is fitted with a custom-built copper parallel plates fixture (diameter of 25 mm) attached to insulating plexiglass sheets. A DC voltage was applied with a DC power supply (Tektronic, PS280) and a custom-built DC power

supply, which can deliver an electric field strength to 2 kV/mm. A digital multimeter (Tektronic, CDM250) was used to monitor voltage and current.

When evaluating the steady state ER response, the electric field was applied for 10 minutes to ensure formation of an equilibrium agglomerate structure before measurements was taken. Each measurement were carried out at a temperature of 25 ± 0.1 °C and repeated at least two or three times.

In these experiments, G' and G" were determined as a function of frequency and electric field strength. Strain sweep tests were first carried out to determine the strain appropriate to measure G' and G" in the linear viscoelastic regime. The appropriate strain was determined to be 0.1% for the electric field strengths of 2, 1, 0.5 kV/mm, 1% for the electric field strengths of 200, 100 V/mm, and 10% for the electric field strengths of 50, 20, 10, 1, 0 V/mm. The deformation frequency was varied from 0.01 to 100 rad/s.

4.4 Results and Discussion

4.4.1 PTAA Characterization

FT-IR spectra of the synthesized PTAA indicated absorption peaks at 2915, 2907, 1703, 1400, 1300-1191, and 835 cm^{-1}, in agreement with literature. These peaks represent the aliphatic C-H stretch, the in-plane thiophene C-H stretch, the carboxylic acid C=O stretch, the thiophene ring stretch, the carboxylic acid C-O stretch, and the out of plane thiophene C-H stretch, respectively (Kim *et al.*, 1999). A dominant feature in the spectrum is a broad O-H absorption at wavenumbers in the range 2400-3400 cm^{-1}, which partially obscures the aliphatic C-H stretch peak.

The ^{1}H-NMR spectrum of PTAA in dueterated DMSO reveals absorption peaks: at 12.35, 7.27- 7.34 and 3.54-3.79 ppm, which can be identified, respectively, as the COOH proton , the thiophene ring protons and the $-CH_2-$ protons of the thiophene ring (Kim *et al.*, 1999).

The UV-Vis spectrum of the synthesized PTAA in DMSO measured shows an absorption peak at 418 nm corresponding to the π-π^* transition of undoped PTAA [25]. For $HClO_4$ doped PTAA, the spectrum possesses two dominant peaks at

372 nm and 475 nm, and a broad peak at 760 nm, which correspond, respectively, to the π-π^* transition of the bipolaron state, the π-π^* transition of the polaron state and the bipolaron transition (Damanze, 1996).

The TGA thermogram of the synthesized PTAA shows two degradation steps at 253°C and 542 °C corresponding to side chain and the backbone degradation, respectively (Radcliffe *et al.*, 1996).

The mean PTAA particle diameter was determined to be approximately 30 μm with a standard deviation of ~ 8 μm. The particle microstructure was observed by scanning electron microscopy (SEM). As shown in Figure 4.1, the shapes of the undoped and doped PTAA particles are quite irregular, and the particles have a broad size distribution.

The specific conductivity of $HClO_4$ doped PTAA was measured by a custom built four-point probe. The conductivity increases with dopant concentration, as shown in Table 4.1. This occurs primarily because of two effects. Increase in dopant concentration causes a corresponding increase in the number of charge carriers, i.e. in the number of polaron and bipolaron species. Also, as the number of charge carriers increases in a PTAA chain, electrostatic repulsion increases the mobility of the charge carriers.

4.4.2 Electrorheological Properties of PTAA/Silicone Systems

The effects of particle concentration and particle conductivity on the electrorheological properties of the suspensions were investigated. Particle concentrations investigated were 10% and 20% by weight (corresponding to volume fraction of 0.048 and 0.092, respectively) at a specific conductivity of 7.5×10^{-2} S/cm (HPT10, and HPT20). To study the effect of conductivity, the particle concentration was fixed at 20% by weight and the particle conductivity values were set at 2.0×10^{-4} and 7.5×10^{-2} S/cm for the LPT20 and HPT20 suspensions, respectively. The dynamic moduli, G' and G", were measured in the linear viscoelastic regime at a strain of 0.1% for the electric field strengths of 2, 1, 0.5 kV/mm, 1% for the electric field strengths of 200, 100 V/mm, and 10% for the

electric field strengths of 50, 20, 10, 1, 0 V/mm as a function of deformation frequency and elapsed time.

4.4.2.1 Effect of Electric Field Strength

Figures 4.2(a) and 4.2(b) show that the dynamic moduli G'(ω) and G"(ω) of the HPT20 suspension increase dramatically by 10 orders of magnitude as the electric field strength is increased through the range 0-2 kV/mm. Close inspection of these results indicates that the system appears to pass through a sol-to-gel transition between 50 and 100V/mm, evidenced by the fact that the storage modulus undergoes a particularly large increase, whereas the loss modulus lags behind. Moreover, at high field strength (1000 V/mm), G' and G" each become essentially frequency independent with G' larger than G" (tan $\delta < 1.0$) at all frequencies. For the HPT10 and LPT20 suspensions, the overall behavior was similar, except that the dynamic moduli were smaller at intermediate field strengths. The increase in the ER response with doping level can be attributed to the enhanced particle polarization due to the increase in particle conductivity (Kim and Park, 2002).

These results are consistent with the generally accepted mechanism for the ER effect in particulate dispersions. Thus, in the absence of the electric field, the particles are randomly dispersed under the influence of the Brownian force. On application of the field, the particles become polarized creating induced dipole moments, leading to interparticle attractions which result in the formation of fibrillar agglomerates in the suspension (Lee *et al.*, 2001). Higher field strength induces a higher dipole moment and increase the strength of the interparticle interactions creating longer agglomerates (Pathasarathy *et al.*, 1994). These longer and stronger agglomerates result in higher rigidity as indicated by a higher G'.

4.4.2.2 Effect of Particle Concentration

Figures 4.3(a) and 4.3(b) compares G' and G" of $HClO_4$ doped PTAA suspensions HPT10 and HPT20 as a function of frequency at field strengths: 0, 100, and 1000 V/mm. In the absence of electric field, at each concentration, G' and G" are of comparable magnitude. The effect of particle concentration becomes apparent at intermediate field strength (100 V/mm), in that the G' and G" values of

the HPT20 suspension are higher than those of HPT10. The ER properties of the HPT systems appear to saturate at a field strength of 1000 V/mm, since G' and G" are independent of particle concentration. This suggests that, at high field strength and high conductivity, the agglomerates size increases to the point that strong interagglomerate interactions lead to a similar network structure at each concentration. Perhaps, at higher concentration, there are more agglomerates, but their sizes are smaller, leading to similar numbers of interagglomerate contacts.

4.4.2.3 Effect of Particle Conductivity

Figures 4.4(a) and 4.4(b) compare G' and G" of $HClO_4$ doped PTAA suspensions LPT20 and HPT20 as a function of frequency at selected field strengths: 0, 100, and 1000 V/mm. The influence of particle conductivity is evident at the intermediate field strength (100 V/mm), in that G' and G" of the HPT20 suspension having higher particle conductivity is substantially larger. The magnitude of the ER effect saturates at highest field strength of 1000 V/mm where G' and G" of LPT20 and HPT20 become comparable in magnitude. Again this leads us to speculate that the high field strength leads to a network structure such that the LPT20 suspension, with lower conductivity has smaller agglomerates, but more of them, resulting in a similar rigidity to that of the HPT20 suspension.

4.4.2.4 Field-driven Sol-to-Gel Transition

The location of the sol-to-gel transition was investigated as the critical field strength where, at low deformation frequency, G' becomes larger than G". In Figure 4.5a, G'(0.01) and G"(0.01), the G' and G" values at a deformation frequency of 0.01 rad/s, are plotted as a function of the applied field strength for the HPT10 and HPT20 suspensions. Each suspension manifests a sol-to-gel transition, defined at the point where G'(0.01) and G"(0.01) crossover each other. For HPT10 the transition occurs at a higher field, 250 V/mm (Figure 4.5a), compared to that for HPT20 (60 V/mm). Thus, as expected, a higher particle concentration correlates to a lower field strength for the transition.

In Figure 4.5(b), G'(0.01) and G"(0.01), are plotted as a function of electric field strength for suspensions LPT20 and HPT20. Again, each suspension shows a transition from fluid-like to solid-like behavior, requiring, however, a higher

critical field strength, 250 V/mm, for the LPT20 suspension having lower particle conductivity.

4.4.2.5 Time Dependence of the ER Response

Finally, we investigate the temporal characteristics of the ER response. Figure 4.6(a) shows the changes in G' of HPT20 suspension, during a time sweep test, in which an electric field was turned on and off alternately. The temporal response of G' was recorded in the linear viscoelastic regime at a strain of 0.1%, and 1 rad/s frequency under various electric field strengths. On applying the electric field, G' immediately increases and rapidly reaches a steady-state value. Subsequently, on turning off the field, G' decreases but does not completely relax to its original value, presumably indicating some irreversible agglomeration, perhaps due to hydrogen bonding between adjacent particles. As with the field-on modulus, the field-off modulus increases with the applied field strength, indicative that the residual interparticle forces are higher when higher fields have been applied. The time required for G' to reach the steady-state value on applying the field is called the induction time, t_{ind}, which was found to be essentially independent of the electric field strength, as shown in Table 4.2. The time required for G' to reach the steady-state value when the field is turned off is called the recovery time, t_{rec}, which increases with increasing field strength, as shown in Table 4.2. The independence of t_{ind} on the field strength may reflect that the solvent is passive to the electric field, and hence the particle diffusivity remains unchanged when the field strength is varied. The increase of t_{rec} with the field strength suggests that longer times are required to disperse larger chain-like structures. It is also found that t_{ind} is independent of concentration or conductivity, whereas t_{rec} is longer at lower concentration and lower conductivity (Table 4.2). Similar behavior to that displayed in Figure 4.6(a) was observed for the HPT10 and LPT20 suspensions, on varying the field strength.

Figure 4.6(b) compares the G' responses of doped PTAA suspensions HPT10, HPT20, and LPT20, at a field strength of 1000 V/mm. It is evident that the field-on values of the modulus vary with concentration and particle conductivity as discussed above. The field-off value of G' and hence the residual agglomeration also show a dependence on particle concentration and conductivity,

being larger at higher concentration and higher conductivity (HPT20 > LPT20 > HPT10).

4.4.2.6 Scaling Analysis

In this section, we carry out a scaling analysis of the ER response of perchloricacid-doped polythiophene suspensions, following the arguments of Parthasarathy and Klingenberg (Parthasarathy and Klingenberg, 1999). These authors carried out a dynamic simulation of linear oscillatory shear flow of ER suspensions, treated as hard, neutrally-buoyant, uncharged dielectric spheres immersed in a dielectric, Newtonian continuous fluid. Application of an electric field polarizes the spheres, in electrostatic interaction between them, and between each sphere and the electrodes. For large particles under large electric fields, colloidal and Brownian forces can be neglected. The equation of motion for particles, neglecting hydrodynamic interactions, can be written as

$$\frac{d\mathbf{r}_i}{dt} = \mathbf{u}^{\infty}(\mathbf{r}_i) + \frac{1}{3\pi\eta_c d}\left[\mathbf{F}_i^{el} + \mathbf{F}_i^{rep}\right] \qquad (4.1)$$

where $\mathbf{r}_i$ is the center position of particle i, $\mathbf{u}^{\infty}(\mathbf{r}_i)$ is the ambient fluid velocity evaluated at the particle center, η_c is the viscosity of the continuous phase, d is the particle diameter, $\mathbf{F}_i^{el}$ is the electrostatic force between particle i and other particles, and $\mathbf{F}_i^{rep}$ is the short-range repulsion between particle i and other particles and between particle i and the electrodes.

The ensemble-averaged electrostatic force exerted on a particle i by particle j in the point-dipole limit is given by

$$\left\langle \mathbf{F}_{ij}^{el} \right\rangle = F_s \left(\frac{d}{r_{ij}}\right)^4 \left[\left(3\cos^2\theta_{ij} - 1\right)\right]\mathbf{e}_r + \sin 2\theta_{ij}\,\mathbf{e}_\theta \qquad (4.2)$$

where

$$F_s = \frac{3}{16}\pi\varepsilon_o\varepsilon_c d^2 E_{rms}^2\left(\beta^*\overline{\beta}^*\right) \qquad (4.3)$$

where r_{ij} is the distance between particle i, which locates at the origin of a spherical coordinate system, and particle j, θ_{ij} is the angle between $\mathbf{e}_z$ axis and $\mathbf{r}_{ij}$, $\varepsilon_o = 8.8542 \times 10^{-12}$ F/m, $\beta^* = (\varepsilon^*_p - \varepsilon^*_c)/(\varepsilon^*_p + 2\varepsilon^*_c)$, the subscript p refers to the particle and the subscript c refers to the continuous medium. $\varepsilon^* = \varepsilon - j\sigma/\varepsilon_o\omega_E$ is the complex dielectric constant, where ε is the relative dielectric constant, σ is the specific conductivity, and ω_E is the angular frequency of the applied electric field, $\mathbf{E} = E_o e^{j\omega_E t}\mathbf{e}_z$. $E_{rms} = E_o / \sqrt{2}$ and β^* is the complex conjugate of β^*. In the low frequency limit ($\omega_E \rightarrow 0$), the force scales as

$$F_s = \frac{3}{16}\pi\varepsilon_o\varepsilon_c d^2 E_{rms}^2 \left(\frac{\sigma_p - \sigma_c}{\sigma_p + 2\sigma_c}\right)^2 \qquad (4.4)$$

and in the high frequency limit ($\omega_E \rightarrow \infty$), the force scales as

$$F_s = \frac{3}{16}\pi\varepsilon_o\varepsilon_c d^2 E_{rms}^2 \left(\frac{\varepsilon_p - \varepsilon_c}{\varepsilon_p + 2\varepsilon_c}\right)^2 \qquad (4.5)$$

The short-range repulsive force between spheres is represented by

$$\mathbf{F}_{ij}^{rep}(r_{ij}) = -F_s \exp\left(-K\frac{r_{ij} - d}{d}\right)\mathbf{e}_r \qquad (4.6)$$

where K is a dimensionless parameter characterizing the magnitude of the repulsive potential.

The sphere/wall interaction is represented by a similar short-range function,

$$\mathbf{F}_{i,wall}^{rep}(r_i) = -F_s \exp\left(-K\frac{h_i - d/2}{d}\right)\mathbf{n} \qquad (4.7)$$

where $h_i = L_z/2 - z_i$, L_z is the electrode gap width, z_i is the distance between particle i and electrode, and $\mathbf{n}$ is the unit normal vector directed from the electrode into the suspension.

The equation of motion can be made dimensionless with the following length, force, and time scales:

$$\ell_{sc} = d, \quad F_{sc} = \frac{3}{16}\pi\varepsilon_o\varepsilon_c d^2\beta^2 E_{rms}^2, \quad t_{sc} = \frac{16\eta_c}{\varepsilon_o\varepsilon_c\beta^2 E_{rms}^2} \qquad (4.8)$$

where

$$\beta^2 \equiv \beta^*\bar{\beta}^*.$$

The equation of motion in dimensionless variables can therefore be written as

$$3\pi\eta_s d \cdot \frac{u_{sc}}{F_{sc}}\left[\frac{d\mathbf{r}_i'(t)}{dt'} - \mathbf{u}'(\mathbf{x}', t')\right] = \mathbf{F}_i^{'el} \qquad (4.9)$$

It follows that the dimensionless rheological responses must be functions of only the dimensionless frequency (Pathasarathy *et al.*, 1994):

$$\frac{G'}{(3/16)\pi\varepsilon_o\varepsilon_c\beta^2 E_o^2} = f_1\left(\frac{16\eta_c\omega}{\varepsilon_o\varepsilon_c\beta^2 E_o^2}\right) \qquad (4.10)$$

$$\frac{G''}{(3/16)\pi\varepsilon_o\varepsilon_c\beta^2 E_o^2} = f_2\left(\frac{16\eta_c\omega}{\varepsilon_o\varepsilon_c\beta^2 E_o^2}\right) \qquad (4.11)$$

Figure 4.7(a) and 4.7(b) show the master plots for G' and G", respectively, obtained by superposing the corresponding data from 20% wt. $HClO_4$-doped PTAA/silicone oil suspensions of high and low conductivities (HPT20 and LPT20). It is evident that the scaled values of the storage and loss moduli for these PTAA suspensions at various electric field strengths and frequency approximately collapse onto a single function of the dimensionless frequency, indicating a moderate success of the model of Parthasarathy and Klingenberg (Parthasarathy *et al.*, 1994).

4.5 Conclusions

In the present study, poly(3-thiophene acetic acid) particles were synthesized via an oxidative polymerization and doped with perchloric acid. The ER properties of the $HClO_4$ doped PTAA/silicone oil suspensions were then investigated by examining the effects of electric field strength, particle concentration, and particle conductivity on the dynamic moduli, G' and G". The results show that G' and G" increase dramatically by 10 orders of magnitude, when the electric field strength is increased to 2 kV/mm. Furthermore, the PTAA based ER fluids exhibited highly viscoelastic behavior under an applied electric field due to the formation of agglomerates induced by the electric polarization within particles. The ER response is enhanced by increasing the electric field strength, the particle concentration, and the particle conductivity. The PTAA suspensions exhibit a transition from fluid-like to solid-like behavior as the field strength is increased. The influence of particle concentration and particle conductivity are most apparent at intermediate field strength, and the suspensions show a saturation in ER properties at a field strength of 1 kV/mm. This suggests a change in the nature of the agglomerate structure at high field strengths and high conductivity and/or concentration, such as network formation. Finally, the frequency-dependent moduli at different electric field strengths and conductivities, when scaled according to the model of Parathasarathy and Klingenberg (Pathasarathy *et al.*, 1994), moderately collapse into single functions of the dimensionless frequency. Of course the latter treatment may be expected to fail under conditions where interagglomerate interactions become important, i.e. in the saturation regime.

4.6 Acknowledgement

The authors would like to acknowledge the financial supports provided by The Thailand Research Fund (TRF) in the RGJ grant no. PHD/0128/2542 and TRF-BGJ grant no. BGJ/03/2544.

4.7 References

Chen, L., Kim, B., Nishino, M., Gong, J., and Osada, Y. (2000). Environmental responses of polythiophene hydrogels. Macromolecules, 33(4), 1232-1236.

Chin, B.D. and Winter, H.H. (2002). Field-induced gelation, yield stress, and fragility of an electro-rheological suspension. Rheol. Acta, 41(3), 265-275.

Cho, M.S. and Choi, H.J. (2000). Scaling analysis of electrorheological poly(naphthalene quinone) radical suspensions. Korea-Australia Rheol. J., 12(3/4), 151-155.

Cho, M.S., Kim, J.W., Choi, H.J., Webber, R.M., and Jhon, M.S. (2000). Electrorheological characteristics of polyaniline and its copolymer suspensions with ionic and nonionic substituents. Colloid Polym. Sci., 278(1), 61-64.

Choi, H.J., Cho, M.S., and Kim, J.W. (2001). Electrorheology and universal yield stress function of semiconducting polymer suspensions. Korea-Australia Rheol. J., 13(4), 197-203.

Demanze, H. (1996). Alternating donor-acceptor substitutions in conjugated polythiophenes. Macromolecules, 29(12), 4267-4273.

Goodwin, J.W., Markham, G.M., and Vincent, B. (1997). Studied on model electrorheological fluids. J. Phys. Chem. B, 101, 1961-1967.

Ha, J.W. and Yang, S.M. (2000). Rheological response of oil-in-oil emulsions in an electric field. J. Rheol., 44(2), 235-256.

Jang, W.H., Kim, J.W., Choi, H.J., and Jhon, M.S. (2001). Synthesis and electrorheology of camphorsulfonic acid doped polyaniline suspensions. Colloid Polym. Sci., 279(8), 823-827.

Jordan, T.C., Shaw, M.T., and McLeish, T.C.B. (1992). Viscoelastic respond of electrorheological fluids: II. Field strength and strain dependence. J. Rheol., 36(3), 441-463.

Jun, J.B., Lee, C.H., Kim, J.W., and Suh, K.D. (2002). Synthesis and characterizations of monodispersed micron-sized polyaniline composite particles for electrorheological fluid materials. Colloid Polym. Sci., 280(8), 744-750.

Kamath, G.M. and Wereley, N. (1997). A nonlinear viscoelastic-plastic model for electrorheological fluids. Smart Mater. Struct., 6, 351-359.

Kim, B., Chen, L., Gong, J., and Osada, Y. (1999). Titration behavior and spectral transitions of water-soluble polythiophene carboxylic acids. Macromolecules, 32(12), 3964-3969.

Kim, S.G., Kim, J.W., Choi, H.J., Suh, M.S., Shin, M.J., and Jhon, M.S. (2000). Synthesis and electrorheological characterization of emulsion-polymerized dodecylbenzenesulfonic acid doped polyaniline-based suspensions. Colloid Polym. Sci., 278(9), 894-898.

Kim, Y.D. and Park, D.H. (2002). The electrorheological responses of suspensions of polypyrrole-coated polyethylene particles. Colloid Polym. Sci., 280(9), 828-834.

Krause, S., and Katherine, B. (2001). Electromechanical response of electrorheological fluids and poly(dimethylsiloxane) networks. Macromolecules, 34(20), 7179-7189.

Lee, H.J., Chin, B.D., Yang, S.M., and Park, O.O. (1998). Surfactant effect on the stability and electrorheological properties of polyaniline particle suspension. J. Colloid Interface Sci., 206, 424-438.

Lee, J.H., Cho, M.S., Choi, H.J., and John, M.S. (1999). Effect of polymerization temperature on polyaniline based electrorheological suspensions. Colloid Polym. Sci., 277(1), 73-76.

Lee Y.H., Kim C.A., Jang W.H., Choi H.J., Jhon M.S. (2001). Synthesis and electrorheological characteristics of microencapsulated polyaniline particles with melamine–formaldehyde resins. Polymer, 42(19), 8277-8283.

Mavroidis, C., Pfeiffer, C., Celestino, C., and Cohen, Y.B. (2000). Controlled compliance haptic interface using electro-rheological fluids. Proceedings of the SPIE Smart Structures Conference, 3987, 1-11.

McLeish, T.C.B., Jordan, T.C., and Shaw, M.T. (1991). Viscoelastic response of electrorheological fluids: I. Frequency dependence. J.Rheol., 35(3), 427-448.

Parthasarathy, M., Ahn, K.H., Belongia, B.M., and Klingenberg, D.J. (1994). The role of suspension structure in the dynamic response of electrorheological

suspensions. Inter. J. Mod. Phys. B, 8(20&21), 2789-2809.

Parthasarathy, M. and Klingenberg, D.J. (1999). Large amplitude oscillatory shear of ER suspensions. J. Non-Newtonain Fluid Mech., 81, 83-104.

Sakurai, R., See, H., Saito, T., Asai, S., and Sumita, M. (1999). Suspension of layered particles: an optimum electrorheological fluid for d.c. applications. Rheol. Acta, 38(5), 478-483.

Sim I.S., Kim J.W., Choi H.J. (2001). Preparation and Electrorheological Characteristics of Poly(*p*-phenylene)-Based Suspensions. Chem. Mater., 13(4), 1243-1247.

Voyles, R.M., Fedder, G., and Khosla, P.K. (1996). Design of a modular tactic sensor and actuator based on an electrorheological gel. Proceeding of the 1996 IEEE International Conference on Robotics and Automation, 13-17.

Table 4.1 Properties of $HClO_4$ doped PTAA suspensions* in silicone oil and electrical conductivity values of PTAA pellets **

Code	Particle concentration (% wt.)	Doping level $[ClO_4]$ / [S]	Specific conductivity (S/cm)	Viscosity, η_o (Pa-s)
HPT10	10	0.255	7.5×10^{-2}	0.244
HPT20	20	0.255	7.5×10^{-2}	0.380
LPT20	20	1.09×10^{-3}	2.0×10^{-4}	0.685

* Particle size distribution was measured by a particle analyzer whose mean and standard deviation are 30 μm and 3 μm, respectively.

** Particle density was 1.97 g/cm^3.

Table 4.2 Induction and recovery times at 25 ± 0.1 °C of $HClO_4$ doped PTAA suspensions under various electric field strengths

System	Electric field strength (V/mm)	t_{ind} (sec)	t_{red} (sec)
HPT20	100	56	840
	500	55	1180
	800	58	1300
	1000	56	1340
HPT10	1000	54	1275
LPT20	1000	54	1290

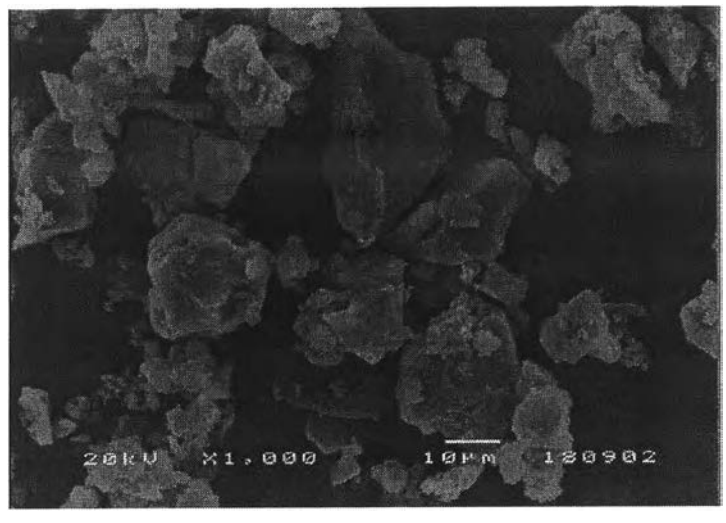

Figure 4.1 Scanning electron microscopy of $HClO_4$ doped polythiophene particles.

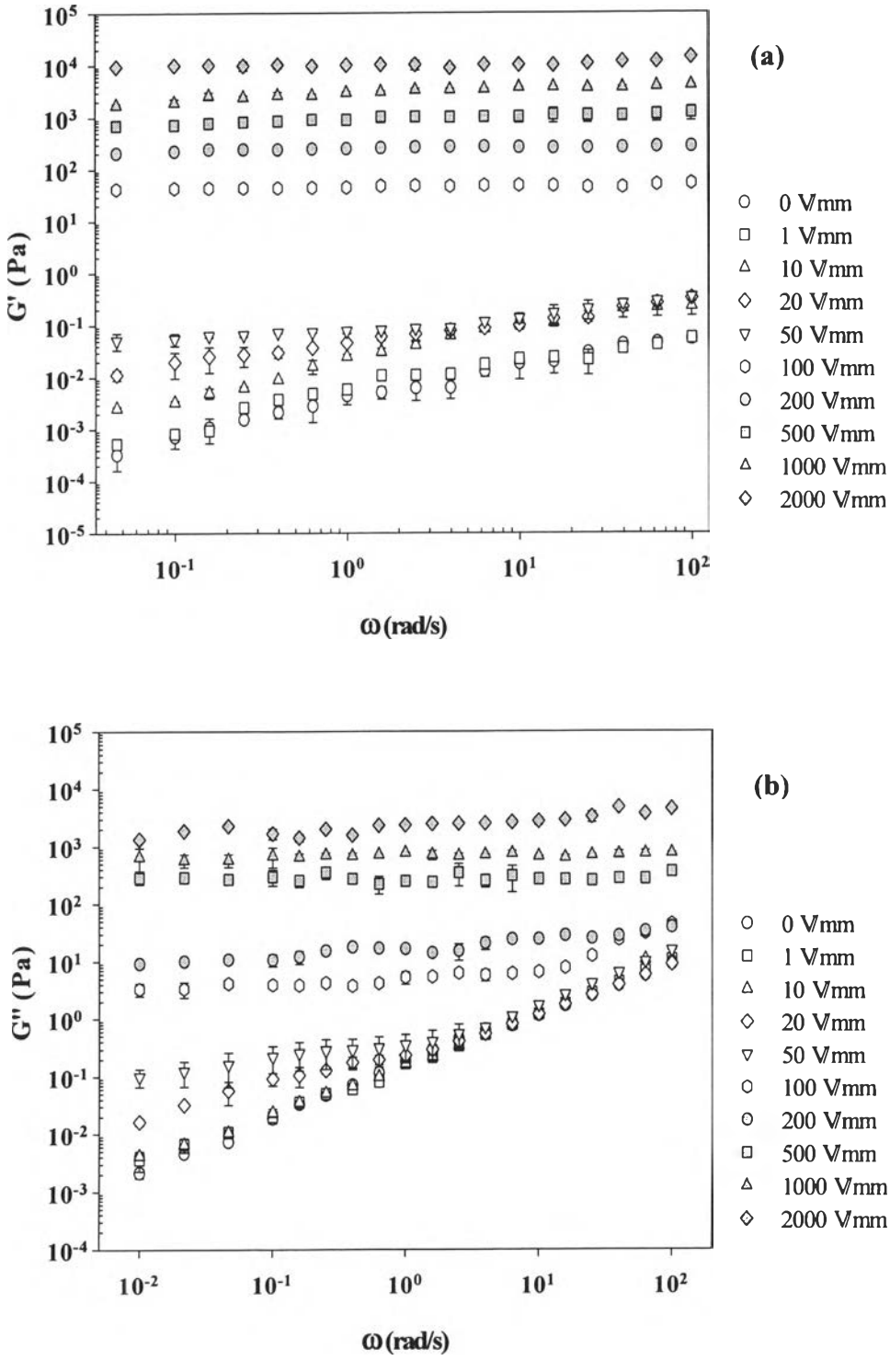

Figure 4.2 Storage and loss moduli of 20% wt. $HClO_4$ highly doped polythiophene/silicone oil suspension (HPT20) at 25 ± 0.1 °C: **(a)** storage moduli G'; **(b)** loss moduli G".

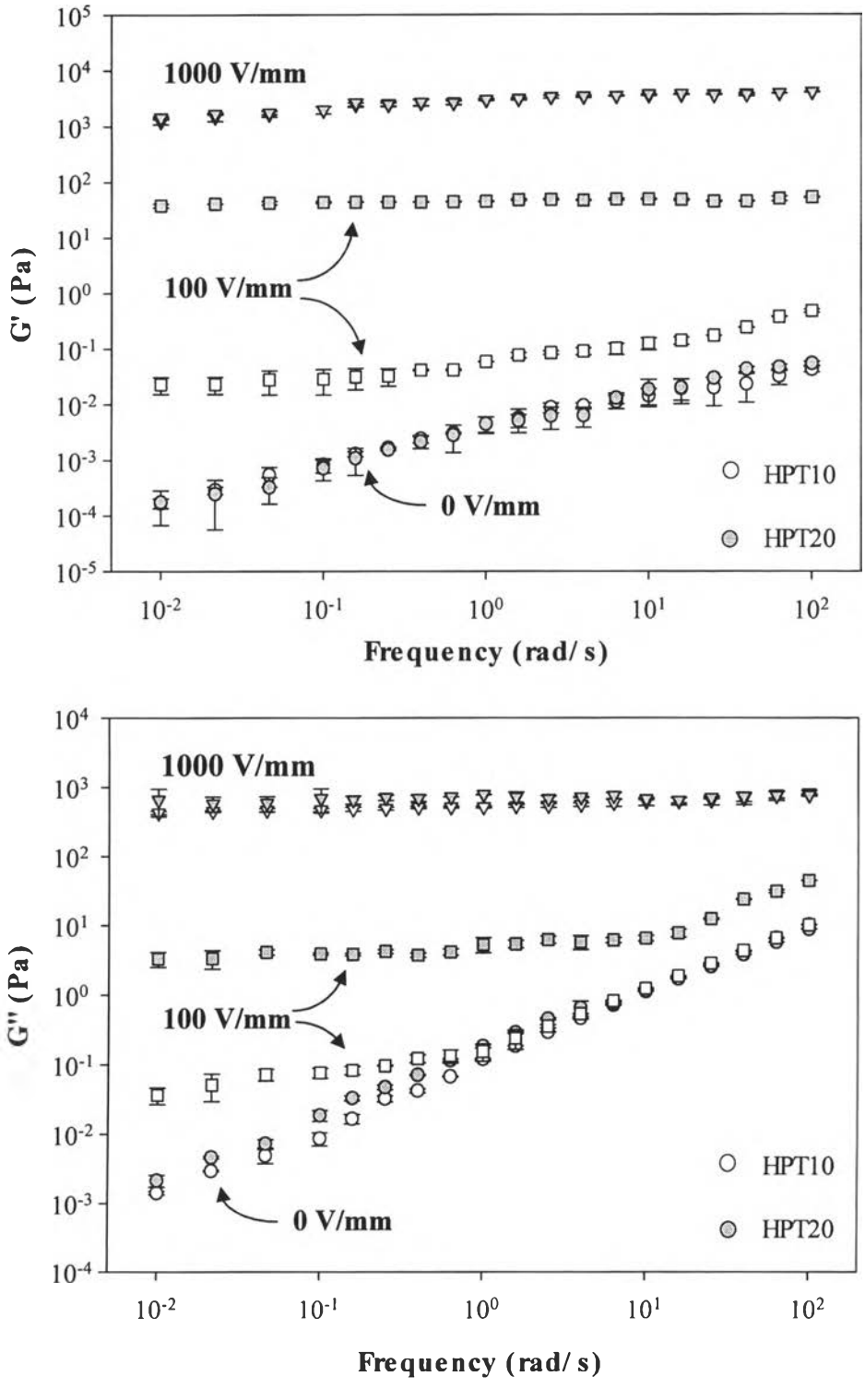

Figure 4.3 Storage and loss moduli of $HClO_4$ highly doped polythiophene/silicone oil suspensions at 25 ± 0.1 °C: **(a)** storage moduli G'; **(b)** loss moduli G".

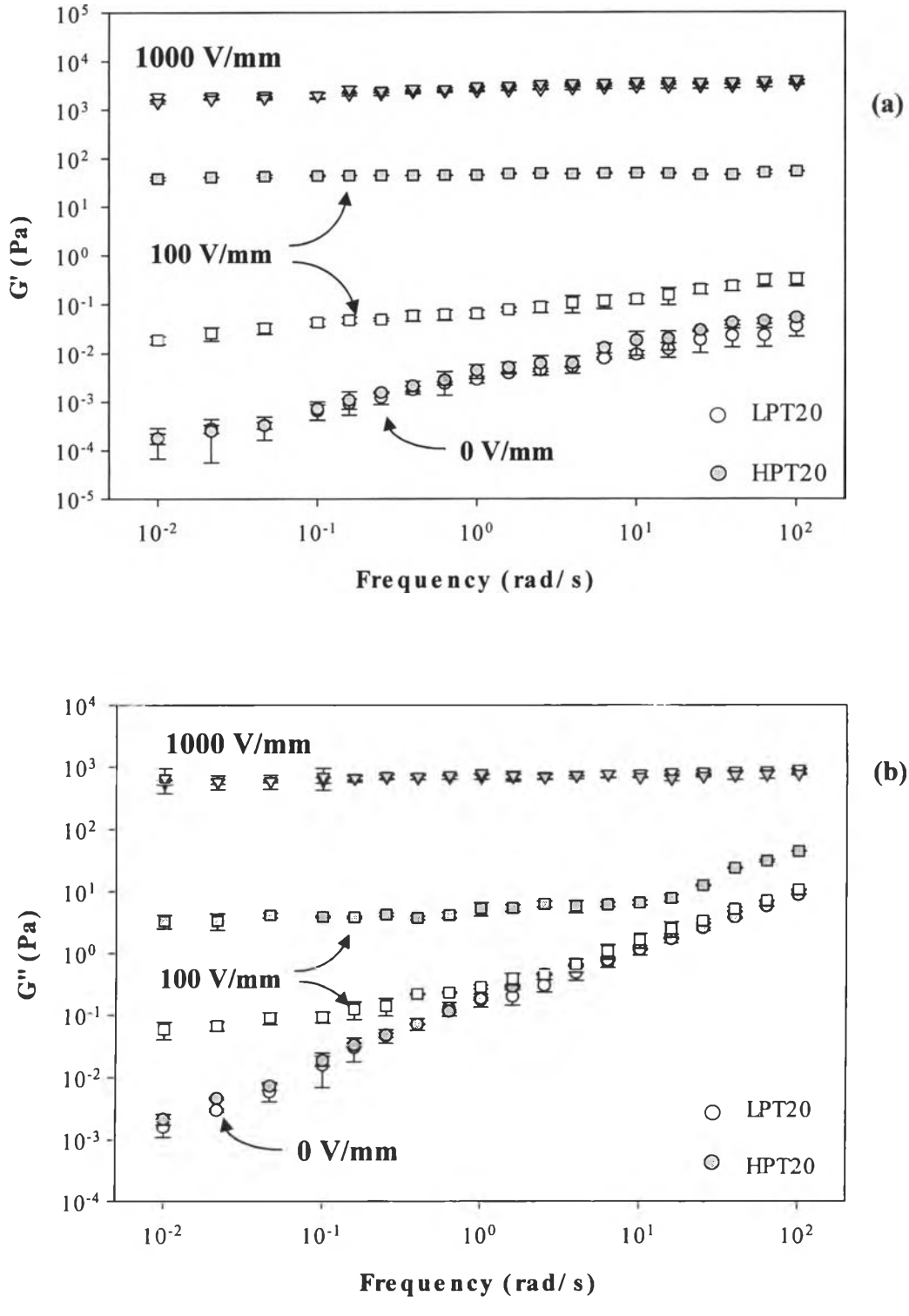

Figure 4.4 Storage and loss moduli of 20% wt. $HClO_4$ doped polythiophene/silicone oil suspensions at temperature of 25 ± 0.1 °C: **(a)** storage moduli G'; **(b)** loss moduli G".

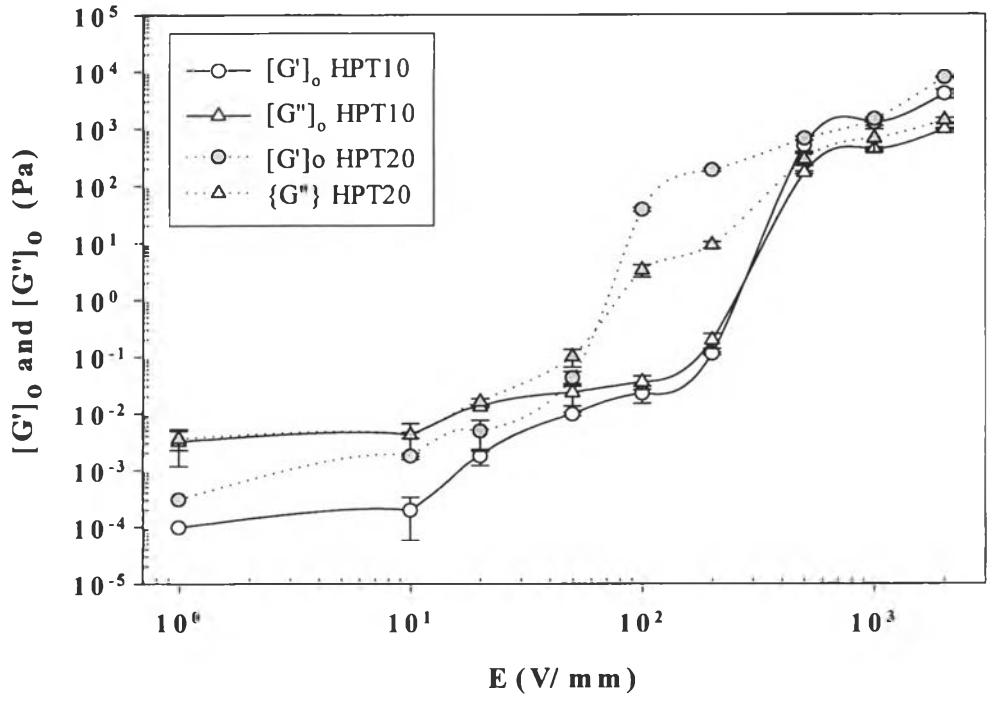

(a)

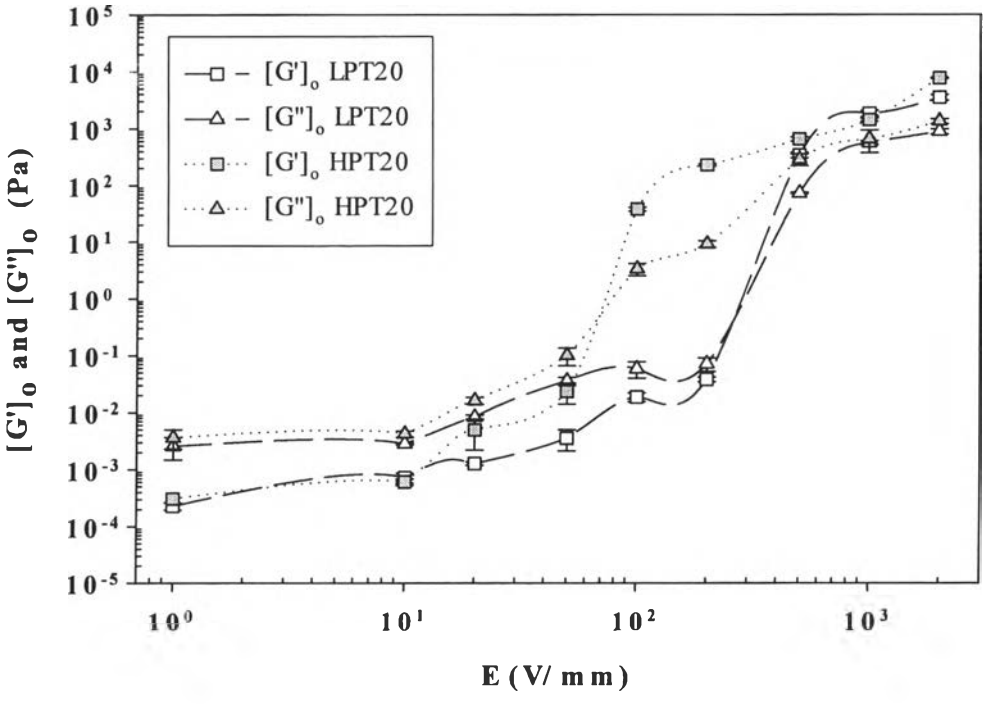

(b)

Figure 4.5 G' and G" values at frequency 0.01 rad/s of $HClO_4$ doped polythiophene/silicone oil suspensions at temperature of 25 ± 0.1 °C: **(a)** highly doped, 10% and 20% wt. and **(b)** lowly doped and highly doped, 20% wt.

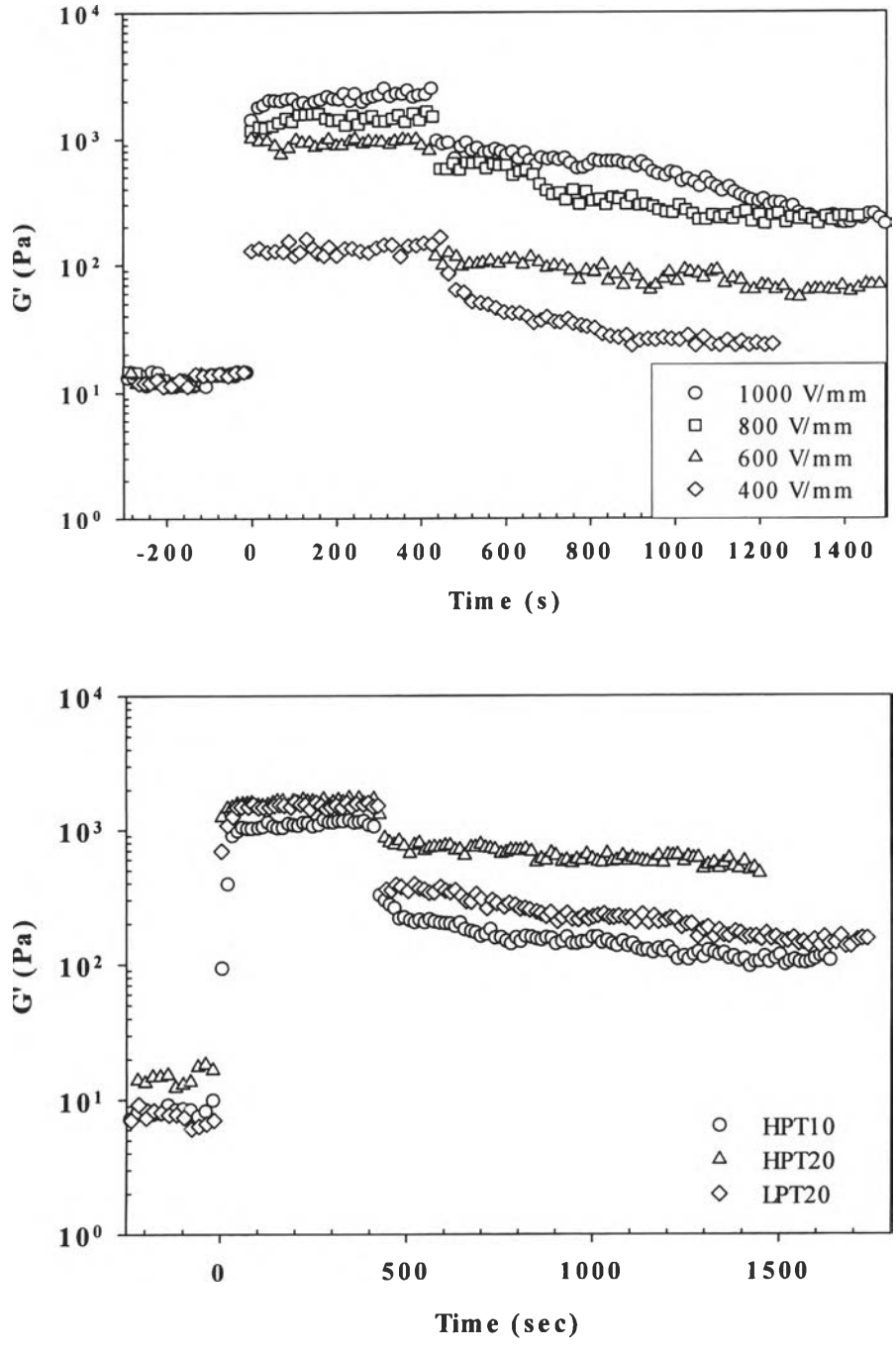

Figure 4.6 Temporal response of storage moduli G' of **(a)** 20% wt. $HClO_4$ highly doped polythiophene/Silicone oil suspension (HPT20) at various electric field strength **(b)** $HClO_4$ doped polythiophene/Silicone oil suspension at electric field strength 1000 V/mm at temperature of 25 ± 0.1 °C.

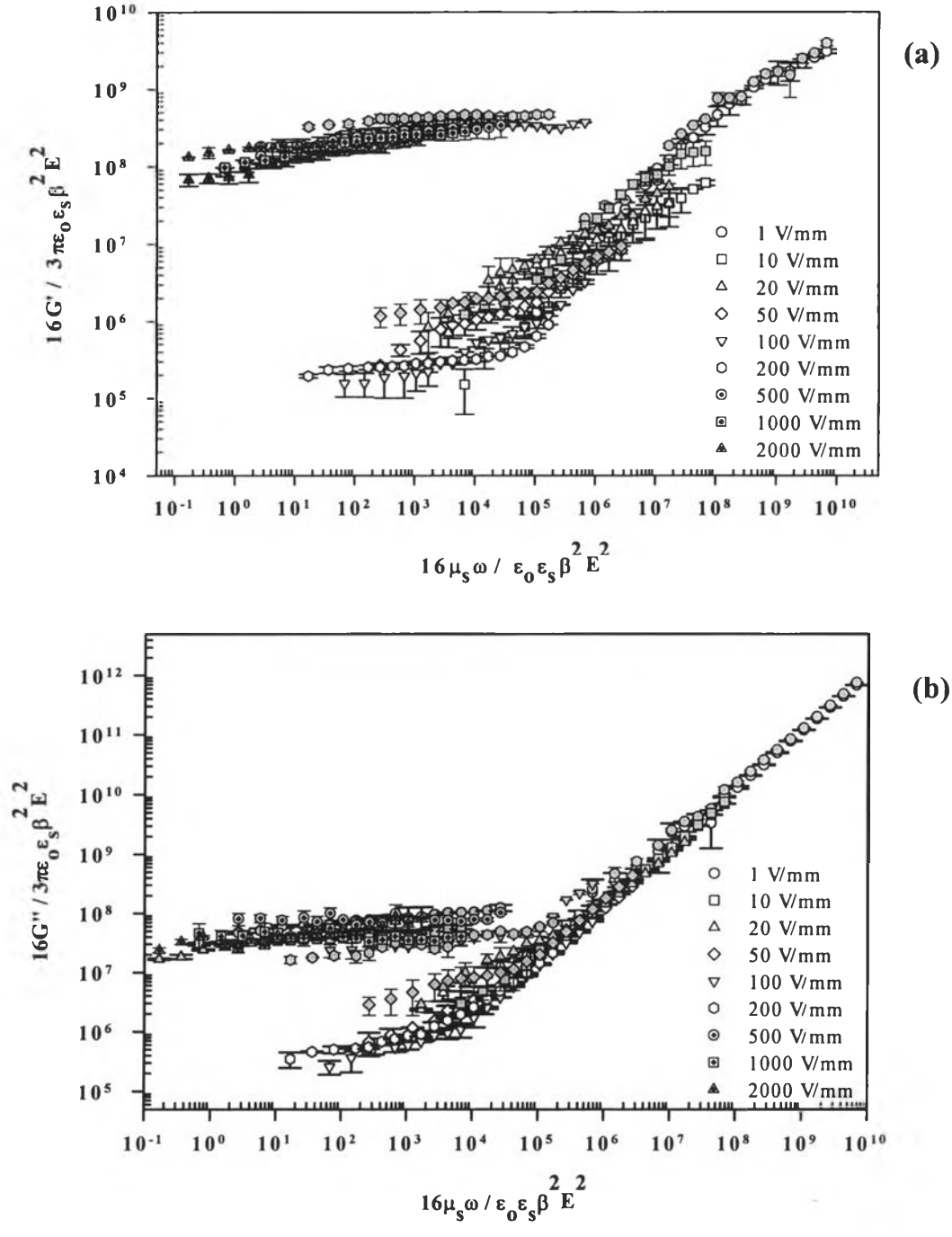

Figure 4.7 Master plot superposing G' and G" data of $HClO_4$ doped polythiophene/silicone oil suspensions at 25 ± 0.1 °C: **(a)** storage moduli G'; **(b)** loss moduli G". Open symbols represent LPT20 and solid symbols represent HPT20. Here ε_o = 8.8542 x 10-2 F/m, ε_s 2.71 F/m, μ_s = 10-4 m2/s, and β = 0.9985 and 0.9999, respectively, for LPT20 and HPT20.